

Persistent-current states originating from the Hilbert space fragmentation in momentum space

Masaya Kunimi^{1,*} and Ippei Danshita^{2,†}

¹*Department of Photo-Molecular Science, Institute for Molecular Science,
National Institutes of Natural Sciences, Myodaiji, Okazaki 444-8585, Japan*

²*Department of Physics, Kindai University, Higashi-Osaka, Osaka 577-8502, Japan*

(Dated: November 3, 2022)

Hilbert space fragmentation (HSF) is a phenomenon that the Hilbert space of an isolated quantum system splits into exponentially many disconnected subsectors. The fragmented systems do not thermalize after long-time evolution because the dynamics are restricted to a small subsector. Inspired by recent developments of the HSF, we construct the Hamiltonian that exhibits the HSF in the momentum space. We show that persistent-current (PC) states emerge due to the HSF in the momentum space. We also investigate the stability of the PC states against the random potential, which breaks the structure of the HSF, and find that the decay rate of the PC is almost independent of the current velocity.

Introduction.— Persistent current (PC) states, which have an infinitely long lifetime, are one of the most counter-intuitive phenomena in quantum many-body physics. These phenomena have been studied in various contexts, such as superfluid helium [1, 2], superconductors [3, 4], mesoscopic physics [5–7], and superfluids of ultracold bosonic and fermionic gases [8–14]. In the case of superconductivity and superfluidity, the macroscopic currents can flow persistently without any external drive. These states cannot be a ground state or thermal equilibrium state [15, 16]. This means that the PC is essentially a kind of nonequilibrium phenomenon.

In superconductors and superfluids, the emergence of PCs can be attributed to the existence of a large energy barrier, which prevents the supercurrent from decaying. In this case, the lifetime of the supercurrent is much longer than the experimental timescales. However, the situation changes when quantum and/or thermal fluctuations are significant in low-dimensional systems. In these situations, the supercurrent decays due to macroscopic quantum tunneling [17–21] and/or thermally activated phase slips [22–24]. The decay rate depends on the current velocity and system temperature [17–20].

The issue of thermalization in isolated quantum many-body systems has become a realistic problem thanks to the developments of various quantum simulators, such as cold atoms or molecules in optical lattices [25–27], Rydberg atoms in optical tweezers [28, 29], trapped ions [30, 31], and superconducting qubits [32–34]. The eigenstate thermalization hypothesis (ETH) is an essential concept of thermalization in isolated systems [35–37]. If the strong version of the ETH is satisfied, i.e., all eigenstates are thermal, the system thermalizes after long-time unitary evolution starting with any initial conditions [38, 39]. It is also known that some systems do not satisfy the strong ETH. Such kinds of systems are referred to as nonergodic systems. Typical examples are quantum integrable systems [40–44] and Anderson or many-body localized systems [45–47]. Recently, quantum many-body

scar [48–52] and Hilbert space fragmentation (HSF) [52–56] have been found as novel ergodicity-broken systems. The HSF occurs due to nontrivial conserved quantities such as dipole operator [54, 55] and domain wall number operator [57, 58]. These operators work as kinetic constraints to the systems. Consequently, the Hilbert space splits into an exponential number of small subsectors, leading to the break down of the ergodicity. The minimum dimension among the fragmented subsectors is one. A subsector with the minimum dimension is referred to as a frozen subsector or frozen state because the dynamics are completely frozen if we choose the frozen state as an initial state.

In this paper, we construct PC states originating from the HSF, inspired by the recent theoretical and experimental understanding of the nonergodic systems. In the typical previous works of the HSF, they implicitly adopted a real-space basis for defining the model Hamiltonian. In this case, the motion of particles or spins in real space is frozen due to kinetic constraints. Instead, we introduce a Hamiltonian which exhibits the HSF in the momentum space. Using the exact diagonalization (ED) method, we numerically show that the HSF indeed occurs in the momentum space. We also show that a PC state can be constructed as a linear combination of a certain couple of the frozen states. We investigate the stability of the PC states against the disorder. We find that the decay rate of the PC states hardly depends on the current velocity, making a clear contrast with the behavior of the conventional PCs.

Model.— We consider soft-core bosons or spinless fermions on a one-dimensional periodic chain. An annihilation (creation) operator at site j is defined by \hat{a}_j (\hat{a}_j^\dagger), where $j = 1, 2, \dots, M$ and M is the number of lattice sites. From the periodic boundary condition, we can introduce the annihilation operator in the momentum space as $\hat{b}_l \equiv (1/\sqrt{M}) \sum_{j=1}^M e^{-2\pi i l j / M} \hat{a}_j$, where $l = 0, 1, \dots, M-1$ is a crystal momentum. For simplicity, we consider an even- M case only.

Here, we construct a model that exhibits the HSF in the momentum space. To do this, recall that if the dipole operator like $\sum_j j \hat{a}_j^\dagger \hat{a}_j$ commutes with the Hamiltonian, the HSF occurs in the real space [54–56]. Naively thinking, we can expect that the Hamiltonian commutes with an operator $\hat{K} \equiv \sum_l l \hat{b}_l^\dagger \hat{b}_l$, the HSF occurs in the momentum space. This might be true, but we want to avoid this situation because \hat{K} breaks space-inversion and time-reversal symmetries. Instead of considering the operator \hat{K} , we consider the operator $\hat{Q} \equiv \sum_{l=0}^{M-1} (l - M/2)^2 \hat{b}_l^\dagger \hat{b}_l$, which preserves the space-inversion and time-reversal symmetries.

First, we consider the kinetic term of the Hamiltonian. It is easily shown that the standard nearest-neighbor hopping hamiltonian $\hat{H}_0 \equiv -J \sum_{j=1}^M (\hat{a}_{j+1}^\dagger \hat{a}_j + \hat{a}_j^\dagger \hat{a}_{j+1}) = -2J \sum_{l=0}^{M-1} \cos(2\pi l/M) \hat{b}_l^\dagger \hat{b}_l$ commutes with \hat{Q} . Therefore, we adopt \hat{H}_0 as a kinetic term of the system. Next, we consider a two-body interaction term \hat{H}_{int} . Let us assume that \hat{H}_{int} has a term $\hat{b}_{l_1}^\dagger \hat{b}_{l_2}^\dagger \hat{b}_{l_4} \hat{b}_{l_3}$. To satisfy the commutation relation $[\hat{Q}, \hat{H}_{\text{int}}] = 0$, $l_{1,2,3,4}$ must satisfy the condition $(l_1 - M/2)^2 + (l_2 - M/2)^2 = (l_3 - M/2)^2 + (l_4 - M/2)^2$. In addition to this requirement, we assume that the interaction Hamiltonian has the space inversion symmetry, i.e., the relation $[\hat{\mathcal{I}}, \hat{H}_{\text{int}}] = 0$ is satisfied. Here $\hat{\mathcal{I}}$ is the space-inversion operator, which is defined by $\hat{\mathcal{I}} \hat{a}_j \hat{\mathcal{I}}^{-1} = \hat{a}_{M-j}$ for real space and $\hat{\mathcal{I}} \hat{b}_l \hat{\mathcal{I}}^{-1} = \hat{b}_{M-l}$ for momentum space. From the above considerations, we adopt the following two-body interaction Hamiltonian that commutes with \hat{Q} and $\hat{\mathcal{I}}$

$$\hat{H}_{\text{int}} = \frac{V}{M} \sum_{s=1}^M (\hat{b}_{M/2+s}^\dagger \hat{b}_{M/2-s-1}^\dagger \hat{b}_{M/2+s+1} \hat{b}_{M/2-s} + \text{h.c.}), \quad (1)$$

where V represents the interaction strength and h.c. denotes the hermitian conjugate. The prefactor $1/M$ is introduced because the total energy should have extensiveness. The total Hamiltonian is given by $\hat{H} \equiv \hat{H}_0 + \hat{H}_{\text{int}}$. In the following, we focus on the soft-core boson case. Qualitatively similar results are obtained for the spinless fermion case. We also emphasize that the interaction Hamiltonian (1) is not a unique choice for satisfying the relation $[\hat{Q}, \hat{H}_{\text{int}}] = 0$. See details for Supplemental Material [59].

Now, we discuss the conserved quantities of the system. By construction, \hat{Q} and $\hat{\mathcal{I}}$ are conserved. Moreover, since there is the $U(1)$ symmetry with respect to the global rotation of the phase of the field operator, the total particle number $\hat{N} \equiv \sum_{j=1}^M \hat{a}_j^\dagger \hat{a}_j = \sum_{l=0}^{M-1} \hat{b}_l^\dagger \hat{b}_l$ is conserved. We define the Hilbert subspace with fixed particle number; $\mathcal{H}_N \equiv \{|\phi\rangle | \hat{N} |\phi\rangle = N |\phi\rangle\}$, where N is the total particle number of the system. We adopt $|\mathbf{n}\rangle \equiv |n_0, n_1, \dots, n_{M-1}\rangle$ as a basis set in \mathcal{H}_N , where $n_l = 0, 1, 2, \dots, N_{\text{max}}$ is an occupation number of the crystal momentum l and N_{max} is the maximum occupation

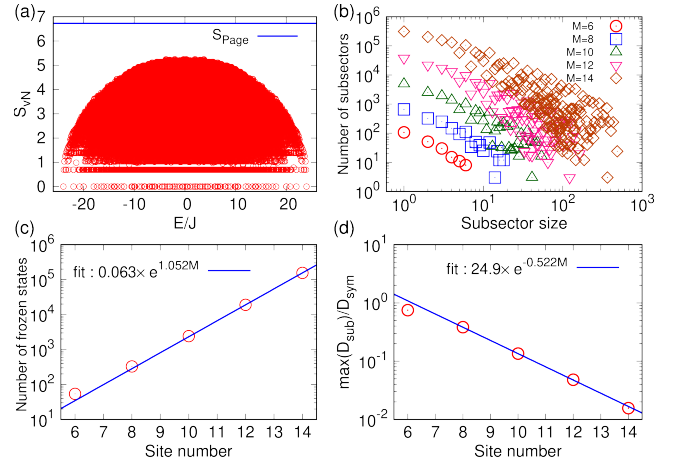


FIG. 1: (a) : von Neumann entanglement entropy as a function of the eigenenergy for $M = N = 12$ and $V = 0.1J$. The dimension of \mathcal{H}_N is 1352078. The blue solid line represents the Page value of the maximum symmetry sector $(N, Q, N_{\text{even}}, \mathcal{I}) = (12, 134, 6, +1)$ whose dimension is 3477. (b) Distribution of the subsystem size for various system sizes. (c) Site number dependence of the number of frozen states. The blue solid line represents the fit to an exponential function. (d) Site number dependence of the ratio between the dimension of the maximum subsystem and dimension of the symmetry sector that belongs to the maximum subsystem. The blue solid line represents the fit to an exponential function

number. In the case of bosons $N_{\text{max}} = N$ whereas in the spinless fermion case $N_{\text{max}} = 1$. In addition to these conserved quantities, $\hat{N}_{\text{even}} \equiv \sum_{l=0,2,\dots} \hat{b}_l^\dagger \hat{b}_l$ is a conserved quantity. Given these four conserved quantities, the symmetry sector is defined by $\mathcal{H}_{N,Q,N_{\text{even}},\mathcal{I}} \equiv \{|\phi\rangle | \hat{N} |\phi\rangle = N |\phi\rangle, \hat{Q} |\phi\rangle = Q |\phi\rangle, \hat{N}_{\text{even}} |\phi\rangle = N_{\text{even}} |\phi\rangle, \hat{\mathcal{I}} |\phi\rangle = \mathcal{I} |\phi\rangle\}$, where Q , N_{even} , and $\mathcal{I} = \pm 1$ are an eigenvalue of \hat{Q} , \hat{N}_{even} , and $\hat{\mathcal{I}}$, respectively. In this paper, we analyze the above system using the ED method [60, 61]. To perform the ED calculations, we use a basis set incorporating the symmetries. We introduce a basis $|\bar{\mathbf{n}}; N, Q, N_{\text{even}}, \mathcal{I}\rangle \equiv [\sqrt{q(\bar{\mathbf{n}})}/2] (|\bar{\mathbf{n}}\rangle + \mathcal{I} \hat{\mathcal{I}} |\bar{\mathbf{n}}\rangle)$, where $|\bar{\mathbf{n}}\rangle$ is the representative state [60, 61] and $|\bar{\mathbf{n}}\rangle$ satisfies $\hat{N} |\bar{\mathbf{n}}\rangle = N |\bar{\mathbf{n}}\rangle, \hat{Q} |\bar{\mathbf{n}}\rangle = Q |\bar{\mathbf{n}}\rangle, \hat{N}_{\text{even}} |\bar{\mathbf{n}}\rangle = N_{\text{even}} |\bar{\mathbf{n}}\rangle$, and $q(\bar{\mathbf{n}})$ is 1 for $\hat{\mathcal{I}} |\bar{\mathbf{n}}\rangle = |\bar{\mathbf{n}}\rangle$ or 2 for $\hat{\mathcal{I}} |\bar{\mathbf{n}}\rangle \neq |\bar{\mathbf{n}}\rangle$. We note that the definition of $q(\bar{\mathbf{n}})$ should be modified in the case of the spinless fermions. See details for Supplemental Material [59].

Results.— Here, we verify that the Hamiltonian (1) exhibits the HSF in the momentum space. Figure 1(a) shows the bipartite entanglement entropy (EE) in the momentum space for $M = N = 12$ [62, 63]. The subsystem $A(B)$ is defined by $l = 0, 1, \dots, M/2 - 1$ ($M/2, M/2 + 1, \dots, M - 1$). We can see a broad distribution of the EE. There are many low-entangled eigenstates even in the center of the spectra. This behavior is in contrast to the ergodic systems. In addition to this property, the maximum value of the EE is significantly lower than the Page value [64]. This is a signature of er-

godicity breaking. To verify the HSF that occurs in this system quantitatively, we investigate the distribution of the subsectors. Figure 1(b) shows the distribution of the subsector size for various system sizes. We find a broad distribution of the subsectors. Here, we focus on the number of the frozen states, whose subsector dimension is one. Figure 1(c) shows the system size dependence of the number of frozen states. We find that the number of frozen states scales as an exponential function of the system size. We also plot the ratio of the maximum dimension of the subsector and dimension of the symmetry sector in Fig. 1(d). The ratio $\max(D_{\text{sub}})/D_{\text{sym}}$ decreases as an exponential function of the system size. This behavior is consistent with the strong version of the HSF [54]. From these results, we conclude that the Hamiltonian (1) exhibits the HSF in the momentum space.

Here, we show that the system has PC states, which have finite current and infinite lifetime. Before discussing the PC states, we define the expression of the current operator \hat{v} :

$$\hat{v} \equiv \hat{v}_{\text{kin}} + \hat{v}_{\text{int}}, \quad (2)$$

$$\hat{v}_{\text{kin}} \equiv \frac{2dJ}{\hbar} \sum_{l=0}^{M-1} \sin\left(\frac{2\pi l}{M}\right) \hat{b}_l^\dagger \hat{b}_l, \quad (3)$$

$$\hat{v}_{\text{int}} \equiv -\frac{idV}{M\hbar} \sum_{s=1}^M \sum_{l=0}^{M-1} (f_{-l} \hat{c}_{s+l}^\dagger \hat{c}_{-s-1+l}^\dagger \hat{c}_{s+1+l} \hat{c}_{-s-l} - \text{h.c.}), \quad (4)$$

$$f_l \equiv \begin{cases} (-1)^l \left[-\frac{1}{2} - \frac{i}{2} \cot(\pi l/M) \right], & l \neq 0 \pmod{M}, \\ -\frac{1}{2}, & l = 0 \pmod{M}, \end{cases} \quad (5)$$

where d is the lattice spacing, $\hat{c}_l \equiv \hat{b}_{M/2+l}$. See the details of the derivation of the above expressions in Supplemental Material [59]. Now, we focus on the frozen states. Because the subsector dimension is one in the frozen subsector, the state $|\bar{\mathbf{n}}; N, Q, N_{\text{even}}, \mathcal{I}\rangle$ is an eigenstate of the Hamiltonian. There are two kinds of frozen states. One is the case $q(\bar{\mathbf{n}}) = 1$. In this case, $|\bar{\mathbf{n}}\rangle$ is an eigenstate of the space inversion operator. From the space inversion symmetry, the current must be zero because the current operator \hat{v} has odd parity under the space inversion, i.e., $\hat{\mathcal{I}}\hat{v}\hat{\mathcal{I}}^{-1} = -\hat{v}$. In the case of $q(\bar{\mathbf{n}}) = 2$, the frozen state is a superposition of $|\bar{\mathbf{n}}\rangle$ and $\hat{\mathcal{I}}|\bar{\mathbf{n}}\rangle$. Utilizing these facts, we can show that the state $|\bar{\mathbf{n}}\rangle$ can have a finite current and infinite lifetime. To show this, we use the relations

$$\begin{aligned} |\bar{\mathbf{n}}\rangle &= \frac{1}{\sqrt{2}} (|\bar{\mathbf{n}}; N, Q, N_{\text{even}}, +1\rangle + |\bar{\mathbf{n}}; N, Q, N_{\text{even}}, -1\rangle) \\ &\equiv \frac{1}{\sqrt{2}} (|+\rangle + |-\rangle). \end{aligned} \quad (6)$$

If we choose the initial condition as $|\psi(0)\rangle = |\bar{\mathbf{n}}\rangle$, the

expectation value of the current operator is given by

$$\langle \psi(t) | \hat{v} | \psi(t) \rangle = \frac{1}{2} e^{i(E_+ - E_-)t/\hbar} \langle + | \hat{v} | - \rangle + \text{c.c.}, \quad (7)$$

where E_\pm is the eigenvalue of the states $|\pm\rangle$. This result implies that if $E_+ = E_-$ and $\langle + | \hat{v} | - \rangle \neq 0$, the expectation value of the current is finite and time-independent. This is equivalent to the PC state. For example, the state $|\mathbf{n}\rangle = |0, N, 0, \dots, 0\rangle$ satisfies the above conditions. We also find that if $E_+ \neq E_-$ and $\langle + | \hat{v} | - \rangle \neq 0$, the expectation value of the current persistently oscillates in time with the period $2\pi\hbar/|E_+ - E_-|$. This is similar to the coherent macroscopic quantum tunneling [65].

Finally, we discuss the stability of the PC states against disorder. Here, we consider two types of disorders. One is the diagonal disorder in the momentum space (or random hopping in the real space). The perturbation Hamiltonian is given by $\hat{H}' \equiv \sum_l T_l \hat{b}_l^\dagger \hat{b}_l \equiv \sum_{j,k} \tilde{T}_{jk} \hat{a}_j^\dagger \hat{a}_k$, where T_l is a real random number and $\tilde{T}_{jk} \equiv (1/M) \sum_l T_l e^{2\pi i l(j-k)/M}$. Owing to the properties of the HSF, if we add a random potential with only diagonal matrix elements in the momentum space, the structure of the HSF preserves. Therefore, the PC states are stable against the diagonal perturbation in the momentum space. On the other hand, the diagonal disorder in the real space (random hopping in the momentum space) breaks the structure of the HSF in the momentum space. We consider the Hamiltonian $\hat{H}_{\text{rand}} \equiv \sum_j U_j \hat{a}_j^\dagger \hat{a}_j = \sum_{l,l'} \tilde{U}_{l-l'} \hat{b}_l^\dagger \hat{b}_l$, where U_j is a real number obeys the uniform distribution on the interval $[-W/2, W/2]$ ($W > 0$) and $\tilde{U}_{l-l'} \equiv (1/M) \sum_j U_j e^{2\pi i(l-l')j/M}$. To investigate the stability of the PC states, we numerically solve the time-dependent Schrödinger equation with the Hamiltonian $\hat{H}_{\text{tot}} \equiv \hat{H} + \hat{H}_{\text{rand}}$ starting with the initial condition $|\psi(0)\rangle = |0, N, 0, \dots, 0\rangle$. We use the Krylov subspace method for calculating the time-evolution operator $e^{-i\hat{H}_{\text{tot}}t/\hbar}$ [66, 67]. The following numerical results are averaged over 750 realizations of the random potential.

Figure 2 shows the time evolution of the current for various disorder strength. As discussed above, the PC states decay after long-time evolution. The decay is faster for the larger disorder strength. This property can be seen in the fidelity shown in Fig. 3, which is defined by the overlap between the initial state $|\psi(0)\rangle$ and the state $|\psi(t)\rangle$. We can see that the decay of the current and that of the fidelity are qualitatively similar. To characterize the timescale of the decay quantitatively, we perform fitting to the fidelity data with a function $Ae^{-\Gamma t}$, where the amplitude A and decay rate Γ are fitting parameters [20]. See details for Supplemental Material [59]. Figure 4 shows the decay rate as a function of the disorder strength. We find that the decay rate is proportional to the disorder strength for the small W region. This is consistent with predictions of Fermi's golden rule. According to Fermi's golden rule, the expression of the decay

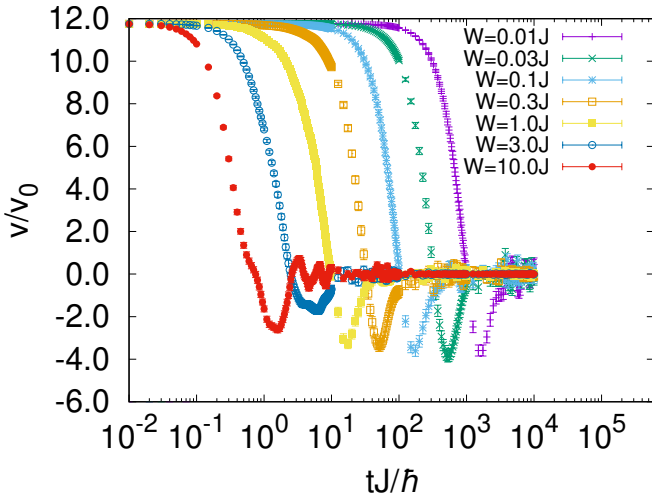


FIG. 2: Expectation value of the current operator \hat{v} for $M = N = 10$ and $V = 0.1J$. The initial condition is $|\psi(0)\rangle = |0, 10, 0, \dots, 0\rangle$. $v_0 \equiv dJ/\hbar$. The error bars represent the standard error of the mean.

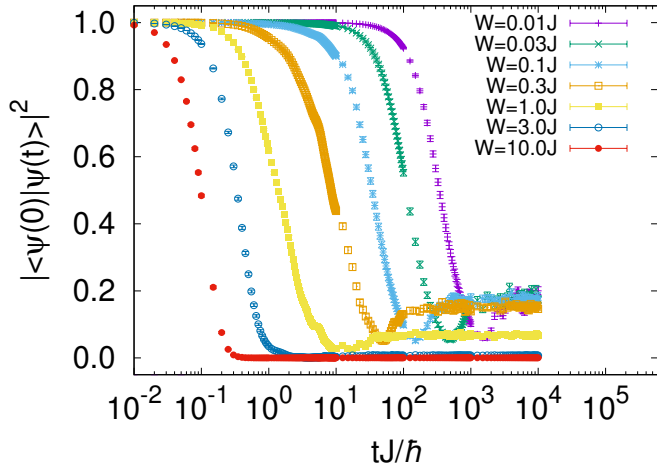


FIG. 3: Fidelity for $M = N = 10$ and $V = 0.1J$. The initial condition is $|\psi(0)\rangle = |0, 10, 0, \dots, 0\rangle$. The error bars represent the standard error of the mean.

rate is given by $\Gamma \propto \sum_n |\langle n | \hat{H}_{\text{rand}} | \psi(0) \rangle|^2 \delta(E_n - E_{\text{ini}})$, where $|n\rangle$ and E_n are the eigenstate and eigenenergy of \hat{H} , respectively, and E_{ini} is the expectation of the non-perturbative energy of the initial state. In the present case, the matrix elements are proportional to W^2 , and the delta function part, which can be interpreted as the density of states, is proportional to $1/W$ [71, 72]. Therefore, the decay rate is proportional to W in the small W region. In the large W region, we can see a clear deviation from the perturbative results. Although we plot $W^{1.5}$ for a guide to the eye, we do not identify the origin of this behavior.

In the end of this section, we discuss the difference between the conventional PC in superfluids and our PC states. There are two main differences. One is its mechanism. In the superfluids, the PC states are protected by

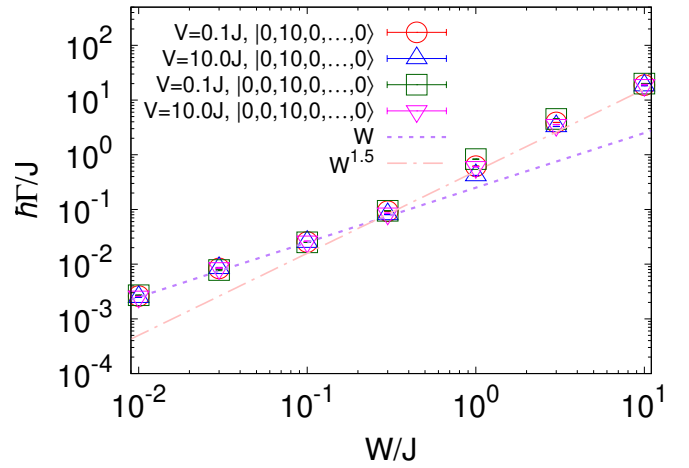


FIG. 4: Decay rate as a function of the disorder strength for $M = N = 10$ and $|\psi(0)\rangle = |0, 10, 0, \dots, 0\rangle$ and $|\psi(0)\rangle = |0, 0, 10, 0, \dots, 0\rangle$. The dotted green and dashed-dotted line represent W and $W^{1.5}$ for a guide to the eye.

the existence of a large energy barrier. This is due to the mean-field nature. On the other hand, the origin of our PC is the kinetic constraints arising from the nontrivial conserved quantity \hat{Q} . This is a purely quantum effect. The other difference is the behavior of the decay rate. For example, in one-dimensional Bose gases, the decay rate depends on the initial state (current) and/or temperature [17, 18, 20, 21, 68–70]. However, our PC states show distinct properties. Figure 4 shows the results for the decay rate as a function of the disorder strength for different initial conditions $|\psi(0)\rangle = |0, N, 0, \dots, 0\rangle$ and $|\psi(0)\rangle = |0, 0, N, 0, \dots, 0\rangle$. This result shows that the decay rate of our PC is insensitive to the initial condition. From these facts, our PC states differ from those originating from superfluidity.

Summary.— To summarize, we constructed the model that exhibits the HSF in the momentum space. The origin of the HSF in the momentum space in our model is the nontrivial conserved quantity \hat{Q} , which works as a kinetic constraint like the dipole operator in the typical HSF case. We verified the HSF in the momentum space by calculating the EE and properties of the distribution of the subsectors. From the properties of the space-inversion symmetry and its matrix elements, we show the existence of the PC states in this system. We investigated the stability of the PC states against the disorder. When the diagonal disorder in the real space is added, the PC decays after long-time evolution. The decay rate of the PC is insensitive to the initial condition. This property manifests that our PC states is different from that of the superfluids or superconductors.

We thank H. Katsura for useful comments. This work was supported by MEXT Quantum Leap Flagship Program (MEXT Q-LEAP) Grant No. JPMXS0118069021 (M.K. and I.D.), JST FOREST Grant No. JPMJFR202T (I.D.), and JSPS KAKENHI Grants No. JP20K14389

(M.K.), No. JP22H05268 (M.K.), No. JP21H01014 (I.D.), and No. JP18H05228 (I.D.).

-
- * Electronic address: kunimi@rs.tus.ac.jp; Present address : Department of Physics, Tokyo University of Science, Shinjuku, Tokyo, 162-8601, Japan
- † Electronic address: danshita@phys.kindai.ac.jp
- [1] J. S. Langer and J. D. Reppy, in *Progress in Low Temperature Physics*, edited by C. J. Gorter (North-Holland, Amsterdam, 1970), Vol. 6, Chap. 1.
- [2] J. D. Reppy, *J. Low Temp. Phys.* **87**, 205 (1992).
- [3] B. S. Deaver and W. M. Fairbank, *Phys. Rev. Lett.* **7**, 43 (1961).
- [4] R. Doll and M. Nábauer, *Phys. Rev. Lett.* **7**, 51 (1961).
- [5] M. Büttiker, Y. Imry, and R. Landauer, *Phys. Lett.* **96A**, 365 (1983).
- [6] V. Chandrasekhar, R. A. Webb, M. J. Brady, M. B. Ketchen, W. J. Gallagher, and A. Kleinsasser, *Phys. Rev. Lett.* **67**, 3578 (1991).
- [7] D. Mailly, C. Chapelier, and A. Benoit, *Phys. Rev. Lett.* **70**, 2020 (1993).
- [8] C. Ryu, M. F. Andersen, P. Cladé, V. Natarajan, K. Helmerson, and W. D. Phillips, *Phys. Rev. Lett.* **99**, 260401 (2007).
- [9] A. Ramanathan, K. C. Wright, S. R. Muniz, M. Zelan, W. T. Hill, C. J. Lobb, K. Helmerson, W. D. Phillips, and G. K. Campbell, *Phys. Rev. Lett.* **106**, 130401 (2011).
- [10] S. Moulder, S. Beattie, R. P. Smith, N. Tammuz, and Z. Hadzibabic, *Phys. Rev. A* **86**, 013629 (2012).
- [11] S. Beattie, S. Moulder, R. J. Fletcher, and Z. Hadzibabic, *Phys. Rev. Lett.* **110**, 025301 (2013).
- [12] A. Kumar, S. Eckel, F. Jendrzejewski, and G. K. Campbell, *Phys. Rev. A* **95**, 021602(R) (2017).
- [13] Y. Cai, D. G. Allman, P. Sabharwal, and K. C. Wright, *Phys. Rev. Lett.* **128**, 150401 (2022).
- [14] G. D. Pace, K. Khani, A. M. Falconi, M. Fedrizzi, N. Grani, D. H. Rajkov, M. Inguscio, F. Scazza, W. J. Kwon, and G. Roati, arXiv:2204.06542 [cond-mat.quant-gas] (2022).
- [15] D. Bohm, *Phys. Rev.* **75**, 502 (1949).
- [16] A. J. Leggett, *Quantum Liquids* (Oxford University Press, Oxford, 2006).
- [17] Yu. Kagan, N. V. Prokof'ev, and B. V. Svistunov, *Phys. Rev. A* **61**, 045601 (2000).
- [18] H. P. Büchler, V. B. Geshkenbein, and G. Blatter, *Phys. Rev. Lett.* **87**, 100403 (2001).
- [19] A. Polkovnikov, E. Altman, E. Demler, B. Halperin, and M. D. Lukin, *Phys. Rev. A* **71**, 063613 (2005).
- [20] I. Danshita and A. Polkovnikov, *Phys. Rev. A* **85**, 023638 (2012).
- [21] I. Danshita, *Phys. Rev. Lett.* **111**, 025303 (2013).
- [22] J. S. Langer and M. E. Fisher, *Phys. Rev. Lett.* **19**, 560 (1967).
- [23] J. S. Langer and V. Ambegaokar, *Phys. Rev.* **164**, 498 (1967).
- [24] D. E. McCumber and B. I. Halperin, *Phys. Rev. B* **1**, 1054 (1970).
- [25] I. Bloch, J. Dalibard, and W. Zwerger, *Rev. Mod. Phys.* **80**, 885 (2008).
- [26] C. Gross and I. Bloch, *Science* **357**, 995 (2017).
- [27] F. Schäfer, T. Fukuhara, S. Sugawa, Y. Takasu, and Y. Takahashi, *Nat. Rev. Phys.* **2**, 411 (2020).
- [28] H. Bernien, S. Schwartz, A. Keesling, H. Levine, A. Omran, H. Pichler, S. Choi, A. S. Zibrov, M. Endres, M. Greiner, V. Vuletić, and M. D. Lukin, *Nature* **551**, 579 (2017).
- [29] A. Browaeys and T. Lahaye, *Nat. Phys.* **16**, 132 (2020).
- [30] R. Blatt and C. F. Roos, *Nat. Phys.* **8**, 277 (2012).
- [31] C. Monroe, W. C. Campbell, L. -M. Duan, Z. -X. Gong, A. V. Gorshkov, P. W. Hess, R. Islam, K. Kim, N. M. Linke, G. Pagano, P. Richerme, C. Senko, and N. Y. Yao, *Rev. Mod. Phys.* **93**, 025001 (2021).
- [32] G. Wendin, *Rep. Prog. Phys.* **80**, 106001 (2017).
- [33] M. Kjaergaard, M. E. Schwartz, J. Braumüller, P. Krantz, J. I.-J. Wang, S. Gustavsson, and W. D. Oliver, *Annu. Rev. Condens. Matter Phys.* **11**, 369 (2020).
- [34] E. Altman, K. R. Brown, G. Carleo, L. D. Carr, E. Demler, C. Chin, B. DeMarco, S. E. Economou, M. A. Eriksson, K.-M. C. Fu, M. Greiner, K. R. A. Hazzard, R. G. Hulet, A. J. Kollár, B. L. Lev, M. D. Lukin, R. Ma, X. Mi, S. Misra, C. Monroe, K. Murch, Z. Nazario, K.-K. Ni, A. C. Potter, P. Roushan, M. Saffman, M. Schleier-Smith, I. Siddiqi, R. Simmonds, M. Singh, I. B. Spielman, K. Temme, D. S. Weiss, J. Vučković, V. Vuletić, J. Ye, and M. Zwerlein, *PRX QUANTUM* **2**, 017003 (2021).
- [35] J. M. Deutsch, *Phys. Rev. A* **43**, 2046 (1991).
- [36] M. Srednicki, *Phys. Rev. E* **50**, 888 (1994).
- [37] M. Rigol, V. Dunjko, and M. Olshanii, *Nature (London)* **452**, 854 (2008).
- [38] L. D'Alessio, Y. Kafri, A. Polkovnikov, and M. Rigol, *Adv. Phys.* **65**, 239 (2016).
- [39] T. Mori, T. N. Ikeda, E. Kaminishi, and M. Ueda, *J. Phys. B: At. Mol. Opt. Phys.* **51**, 112001 (2018).
- [40] M. Rigol, V. Dunjko, V. Yurovsky, and M. Olshanii, *Phys. Rev. Lett.* **98**, 050405 (2007).
- [41] M. Rigol, *Phys. Rev. Lett.* **103**, 100403 (2009)
- [42] M. Rigol, *Phys. Rev. A* **80**, 053607 (2009).
- [43] A. C. Cassidy, C. W. Clark, and M. Rigol, *Phys. Rev. Lett.* **106**, 140405 (2011)
- [44] L. Vidmar and M. Rigol, *J. Stat. Mech.:Theory Exp.* **2016** 064007.
- [45] R. Nandkishore and D. A. Huse, *Ann. Rev. Condens. Matter Phys.* **6**, 15 (2015).
- [46] E. Altman and R. Vosk, *Annu. Rev. Condens. Matter Phys.* **6**, 383 (2015).
- [47] D. A. Abanin, E. Altman, I. Bloch, and M. Serbyn, *Rev. Mod. Phys.* **91**, 021001 (2019).
- [48] C. J. Turner, A. A. Michailidis, D. A. Abanin, M. Serbyn, and Z. Papić, *Nat. Phys.* **14**, 745 (2018).
- [49] C. J. Turner, A. A. Michailidis, D. A. Abanin, M. Serbyn, and Z. Papić, *Phys. Rev. B* **98**, 155134 (2018).
- [50] Z. Papić, arXiv:2108.03460 (2021).
- [51] M. Serbyn, D. A. Abanin, and Z. Papić, *Nat. Phys.* **17**, 675 (2021).
- [52] S. Moudgalya, B. A. Bernevig, and N. Regnault, *Rep. Prog. Phys.* **85**, 086501 (2022).
- [53] G. De Tomasi, D. Hetterich, P. Sala, and F. Pollmann, *Phys. Rev. B* **100**, 214313 (2019).
- [54] P. Sala, T. Rakovszky, R. Verresen, M. Knap, and F. Pollmann, *Phys. Rev. X* **10**, 011047 (2020).
- [55] V. Khemani, M. Hermele, and R. Nandkishore, *Phys. Rev. B* **101**, 174204 (2020).
- [56] S. Moudgalya, A. Prem, R. Nandkishore, N. Regnault, and B. A. Bernevig, *Memorial Volume for Shoucheng*

- Zhang* (World Scientific, 2021), pp. 147-209.
- [57] Z.-C. Yang, F. Liu, A. V. Gorshkov, and T. Iadecola, *Phys. Rev. Lett.* **124**, 207602 (2020).
- [58] A. Yoshinaga, H. Hakoshima, T. Imoto, Y. Matsuzaki, and R. Hamazaki, *Phys. Rev. Lett.* **129**, 090602 (2022).
- [59] See Supplemental Material at url.
- [60] A. W. Sandvik, in *Lectures on the Physics of Strongly Correlated Systems XIV: Fourteenth Training Course in the Physics of Strongly Correlated Systems*, edited by A. Avella and F. Mancini, AIP Conf. Proc. No. 1297, (AIP, New York, 2010), p 135.
- [61] J.-H. Jung and J. D. Noh, *J. Korean Phys. Soc.* **76**, 670 (2020).
- [62] R. Lundgren, J. Blair, M. Greiter, A. Läuchli, G. A. Fiete, and R. Thomale, *Phys. Rev. Lett.* **113**, 256404 (2014).
- [63] F. Schindler, N. Regnault, and B. A. Bernevig, *Phys. Rev. B* **105**, 035146 (2022).
- [64] D. N. Page, *Phys. Rev. Lett.* **71**, 1291 (1993).
- [65] I. Danshita and A. Polkovnikov, *Phys. Rev. B* **82**, 094304 (2010).
- [66] M. Hochbruck and C. Lubich, *SIAM J. NUMER. ANAL.* **34**, 1911 (1997).
- [67] S. Paeckel, T. Köhler, A. Swoboda, S. R. Manmana, U. Schollwöck, and C. Hubig, *Ann. Phys. (N. Y.)* **411**, 167998 (2019).
- [68] C. D. Fertig, K. M. O'Hara, J. H. Huckans, S. L. Rolston, W. D. Phillips, and J. V. Porto, *Phys. Rev. Lett.* **94**, 120403 (2005).
- [69] L. Tanzi, S. S. Abbate, F. Cataldini, L. Gori, E. Lucioni, M. Inguscio, G. Modugno, and C. D'Errico, *Sci. Rep.* **6**, 25965 (2016).
- [70] M. Kunimi and I. Danshita, *Phys. Rev. A* **95**, 033637 (2017).
- [71] E. J. Torres-Herrera, M. Vyas, and L. F. Santos, *New J. Phys.* **16**, 063010 (2014).
- [72] G. De Tomasi, M. Amini, S. Bera, I. M. Khaymovich, and V. E. Kravtsov, *SciPost Phys.* **6**, 014 (2019).

SUPPLEMENTAL MATERIAL FOR PERSISTENT-CURRENT STATES ORIGINATING FROM THE HILBERT SPACE FRAGMENTATION IN MOMENTUM SPACE

GENERALIZATION OF THE HAMILTONIAN

In the main text, we discuss the Hilbert space fragmentation (HSF) in the momentum space for the specific Hamiltonian. The Hamiltonian is constructed to satisfy the commutation relations

$$[\hat{N}, \hat{H}] = 0, [\hat{Q}, \hat{H}] = 0, [\hat{N}_{\text{even}}, \hat{H}] = 0, [\hat{\mathcal{I}}, \hat{H}] = 0, \quad (8)$$

where \hat{N} , \hat{Q} , \hat{N}_{even} , and $\hat{\mathcal{I}}$ are defined in the main text. Here, we show that more general form of the Hamiltonian also satisfies the commutation relations (8) and exhibits the HSF in the momentum space.

We can check that the following Hamiltonians satisfies the commutation relations (8):

$$\hat{H}^{(i)} \equiv \hat{H}'_0 + \hat{H}_{\text{int}}^{(i)}, \quad (i = 1, 2, 3), \quad (9)$$

$$\hat{H}'_0 \equiv \sum_{l=0}^{M-1} \epsilon_l \hat{n}_l, \quad (10)$$

$$\hat{H}_{\text{int}}^{(1)} \equiv \sum_{r=1}^{M/2} \frac{V_r^{(1)}}{M} \sum_{s=1}^M (\hat{b}_{M/2+s}^\dagger \hat{b}_{M/2-s-r}^\dagger \hat{b}_{M/2+s+r} \hat{b}_{M/2-s} + \hat{b}_{M/2-s}^\dagger \hat{b}_{M/2+s+r}^\dagger \hat{b}_{M/2-s-r} \hat{b}_{M/2+s}), \quad (11)$$

$$\hat{H}_{\text{int}}^{(2)} \equiv \sum_{r=1}^{M/2} \frac{V_r^{(2)}}{M} \sum_{s=1}^M (\hat{b}_{M/2+s}^\dagger \hat{b}_{M/2+s+r}^\dagger \hat{b}_{M/2-s-r} \hat{b}_{M/2-s} + \hat{b}_{M/2-s}^\dagger \hat{b}_{M/2-s-r}^\dagger \hat{b}_{M/2+s+r} \hat{b}_{M/2+s}), \quad (12)$$

$$\hat{H}_{\text{int}}^{(3)} \equiv \sum_{r=1}^{M/2} \frac{V_r^{(3)}}{M} \sum_{s=1}^M (\hat{b}_{M/2+s}^\dagger \hat{b}_{M/2+s+r}^\dagger \hat{b}_{M/2+s+r} \hat{b}_{M/2-s} + \hat{b}_{M/2-s}^\dagger \hat{b}_{M/2+s+r}^\dagger \hat{b}_{M/2+s+r} \hat{b}_{M/2+s}), \quad (13)$$

where \hat{b}_l and \hat{b}_l^\dagger are the operator of the soft-core boson or spinless fermion, $\epsilon_l = \epsilon_{M-l} \in \mathbb{R}$ is the single-particle dispersion and $V_r^{(1,2,3)} \in \mathbb{R}$ represents the interaction strength. If we choose $\epsilon_l = -2J \cos(2\pi l/M)$ and $V_r^{(1)} = V \delta_{r,1}$, the Hamiltonian (11) reduces to that used in the main text.

For reference, we show the real-space representation of the Hamiltonian $\hat{H}^{(i)}$. The results are as follows:

$$\hat{H}'_0 = \sum_{j,k} \tilde{c}_{j,k} \hat{a}_j^\dagger \hat{a}_k, \quad (14)$$

$$\tilde{c}_{j,k} \equiv \frac{1}{M} \sum_{l=0}^{M-1} \epsilon_l e^{2\pi i l(j-k)/M}, \quad (15)$$

$$\hat{H}_{\text{int}}^{(1)} = \sum_{r=1}^{M/2} \frac{2V_r^{(1)}}{M^2} \sum_{j_1, j_2, j_3, j_4} \delta_{j_1 - j_2 + j_3 - j_4, 0 \bmod M} (-1)^{j_1 + j_2 - j_3 - j_4} \cos \left[\frac{2\pi(j_2 + j_4)r}{M} \right] \hat{a}_{j_1}^\dagger \hat{a}_{j_2}^\dagger \hat{a}_{j_4} \hat{a}_{j_3}, \quad (16)$$

$$\hat{H}_{\text{int}}^{(2)} = \sum_{r=1}^{M/2} \frac{2V_r^{(2)}}{M^2} \sum_{j_1, j_2, j_3, j_4} \delta_{j_1 + j_2 + j_3 + j_4, 0 \bmod M} (-1)^{j_1 + j_2 - j_3 - j_4} \cos \left[\frac{2\pi(j_2 + j_3)r}{M} \right] \hat{a}_{j_1}^\dagger \hat{a}_{j_2}^\dagger \hat{a}_{j_4} \hat{a}_{j_3}, \quad (17)$$

$$\hat{H}_{\text{int}}^{(3)} = \sum_{r=1}^{M/2} \frac{2V_r^{(3)}}{M^2} \sum_{j_1, j_2, j_3, j_4} \delta_{j_1 + j_2 + j_3 - j_4, 0 \bmod M} (-1)^{j_1 + j_2 - j_3 - j_4} \cos \left[\frac{2\pi(j_2 - j_4)r}{M} \right] \hat{a}_{j_1}^\dagger \hat{a}_{j_2}^\dagger \hat{a}_{j_4} \hat{a}_{j_3}, \quad (18)$$

where $\delta_{x, 0 \bmod M} = 1$ if $x = 0 \bmod M$ otherwise 0. From the above expressions, we can easily see that the system breaks the translational symmetry.

As an example, we consider the Hamiltonian (11) with $\epsilon_l = -2J \cos(2\pi l/M)$ and $V_r^{(1)} = V$ ($r \leq r_{\text{max}}$) and otherwise 0 for the soft-core bosons. When $r_{\text{max}} = 1$, this Hamiltonian coincides with that in the main text. Figure 5 shows the numerical results of the von Neumann entanglement entropy, distribution of the subsector size, the number of frozen states, and $\max(D_{\text{sub}})/D_{\text{sym}}$ for $V = 0.1J$ and $r_{\text{max}} = 6$, respectively. We can find that the qualitative behavior is almost the same as that shown in Fig. 1. This indicates that the other form of the Hamiltonian also exhibits the HSF in the momentum space. Figure 6 shows the system size dependence of the number of the frozen states for various r_{max} . These results suggest that the number of frozen states decreases for increasing r_{max} . The reason for this behavior is that the increase in r_{max} increases the number of the off-diagonal elements of the Hamiltonian. Although the number of the frozen states becomes small for large r_{max} , the system size dependence is still exponential. This means that the strong version of the HSF still survives, even in the case of a finite interaction range.

RESULTS FOR SPINLESS FERMIONS

In this section, we discuss the HSF in the momentum space for spinless fermions. Before showing the numerical results, we mention the definition of the space-inversion operator for spinless fermion case. In this case, owing to the Fermionic sign, we obtain

$$\hat{\mathcal{I}}|\mathbf{n}\rangle = \hat{\mathcal{I}}|n_0, n_1, \dots, n_{M-1}\rangle = (-1)^{S(\mathbf{n})} |n_0, n_{M-1}, n_{M-2}, \dots, n_2, n_1\rangle, \quad (19)$$

$$S(\mathbf{n}) \equiv \frac{1}{2}(N - n_0)(N - n_0 - 1). \quad (20)$$

From this result, when $q(\bar{\mathbf{n}}) = 1$, we have $\hat{\mathcal{I}}|\bar{\mathbf{n}}\rangle = \pm|\bar{\mathbf{n}}\rangle$ in contrast to the bosonic case. For example, $\hat{\mathcal{I}}|0, 1, 0, 1\rangle = -|0, 1, 0, 1\rangle$ and $\hat{\mathcal{I}}|1, 0, 1, 0\rangle = |1, 0, 1, 0\rangle$ hold. Therefore, we define $q(\bar{\mathbf{n}}) = 1$ for $\hat{\mathcal{I}}|\bar{\mathbf{n}}\rangle = \pm|\bar{\mathbf{n}}\rangle$ and $q(\bar{\mathbf{n}}) = 2$ for $\hat{\mathcal{I}}|\bar{\mathbf{n}}\rangle \propto \mp|\bar{\mathbf{n}}\rangle$.

Here, we show the exact diagonalization results for the spinless fermion Hamiltonian. The Hamiltonian is the same as the main text, except that the operators are spinless fermions. Figure 7 shows the numerical results of the von Neumann entanglement entropy, distribution of the subsector size, the number of frozen states, and $\max(D_{\text{sub}})/D_{\text{sym}}$ for $V = 0.1J$, $M = 26$, and $N = 13$. We find that all results are qualitatively the same as the case of the soft-core bosons. Therefore, we conclude that the HSF in the momentum space also occurs in the case of the spinless fermion.

DERIVATION OF THE CURRENT OPERATOR

Our Hamiltonian has nontrivial interaction terms. As a result, the current operator from the interaction part exists. Here, we derive the expression of the current operator. To do this, we introduce the Hamiltonian with a uniform

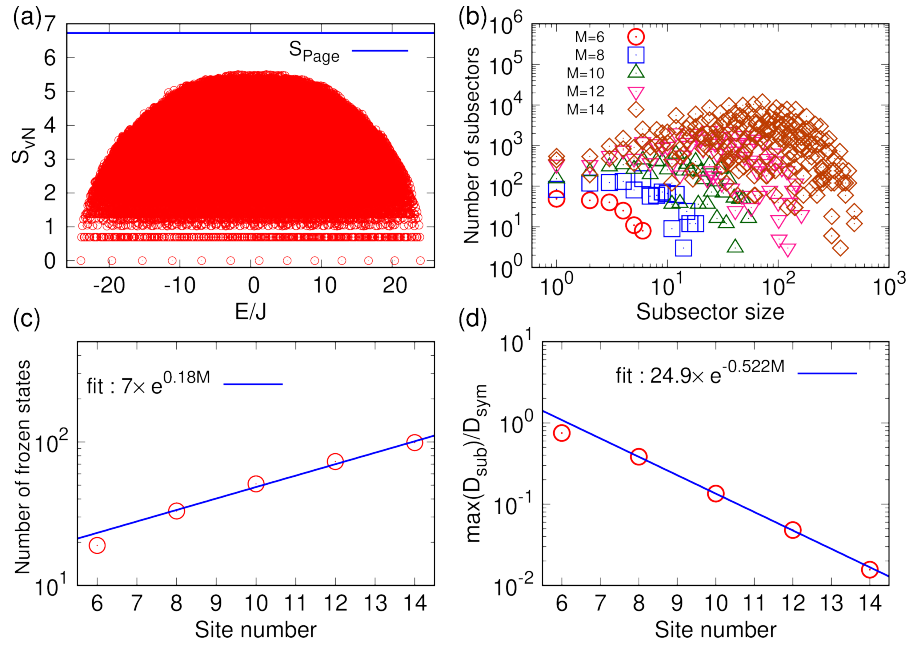


FIG. 5: (a) : von Neumann entanglement entropy as a function of the eigenenergy for $M = N = 12$, $r_{\max} = 6$, and $V = 0.1J$. The dimension of \mathcal{H}_N is 1352078. The blue solid line represents the Page value of the maximum symmetry sector $(N, Q, N_{\text{even}}, \mathcal{I}) = (12, 134, 6, +1)$ whose dimension is 3477. (b) Distribution of the subsector size for various system sizes. (c) Site number dependence of the number of frozen states. The blue solid line represents the fit to an exponential function. (d) Site number dependence of the ratio between the dimension of the maximum subsector and dimension of the symmetry sector that belongs to the maximum subsector. The blue solid line represents the fit to an exponential function.

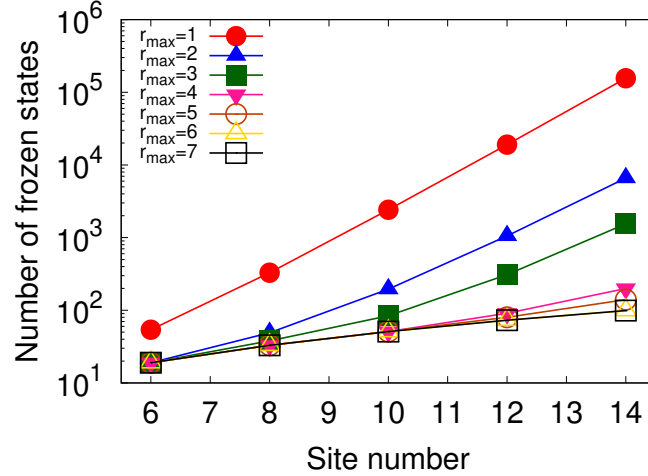


FIG. 6: System size dependence of the number of frozen states for $V = 0.1J$ and $r_{\max} = 1 \sim 7$.

phase twist:

$$\hat{H}(\theta) \equiv \hat{U}^\dagger(\theta) \hat{H} \hat{U}(\theta), \quad (21)$$

$$\hat{U}(\theta) \equiv e^{-i\theta \hat{X}}, \quad (22)$$

$$\hat{X} \equiv \sum_{j=1}^M j \hat{a}_j^\dagger \hat{a}_j, \quad (23)$$

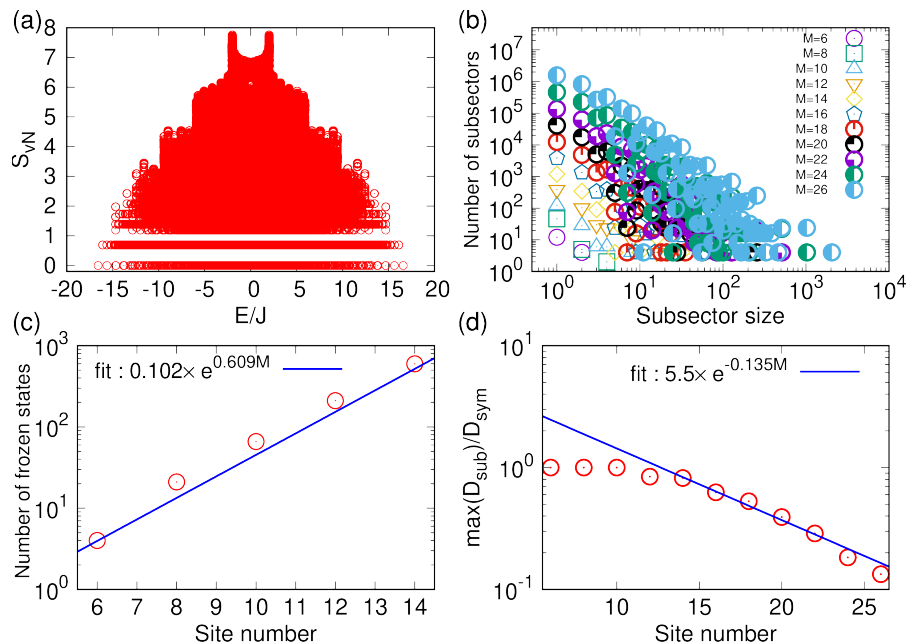


FIG. 7: (a) : von Neumann entanglement entropy as a function of the eigenenergy for $M = 26$ and $N = 13$, and $V = 0.1J$ for spinless fermion Hamiltonian. The dimension of \mathcal{H}_N is 10400600. (b) Distribution of the subsector size for various system sizes. The particle number is fixed to $N = M/2$. (c) Site number dependence of the number of frozen states. The blue solid line represents the fit to an exponential function. (d) Site number dependence of the ratio between the dimension of the maximum subsector and dimension of the symmetry sector that belongs to the maximum subsector.

where θ is a real number. From Eqs. (22) and (23), the following relation holds: $\hat{U}^\dagger(\theta)\hat{a}_j\hat{U}(\theta) = e^{-i\theta j}\hat{a}_j$. The current operator is defined by

$$\hat{v} \equiv -\frac{d}{\hbar} \left. \frac{\partial \hat{H}(\theta)}{\partial \theta} \right|_{\theta=0}. \quad (24)$$

Using this definition, we obtain the expression of the current operator (3) and (4).

DETAILS OF THE FITTING OF THE DECAY RATE

Here, we explain how to extract the decay rate from the fitting to the fidelity. To perform the fitting to the fidelity properly, we need to specify the fitting region. For short time regime, the fidelity can be written as

$$|\langle \psi(0) | \psi(t) \rangle|^2 \simeq 1 - \left[\langle \psi(0) | \hat{H}^2 | \psi(0) \rangle - \langle \psi(0) | \hat{H} | \psi(0) \rangle^2 \right] \frac{t^2}{\hbar^2}. \quad (25)$$

This means that the fidelity for the short time region is determined by the variance of the energy. We can also show that the long-time average of the fidelity converges to the inverse partition ratio [1]. In the long time regime, the fidelity fluctuates around this value. To extract the exponential decay, appropriate choice of the fitting region is required.

Figure 8 shows an example of the fitting region. We summarize the fitting region $[t_1, t_2]$ as a function of the disorder strength in Table I. We used these values to obtain the data shown in Fig. 4.

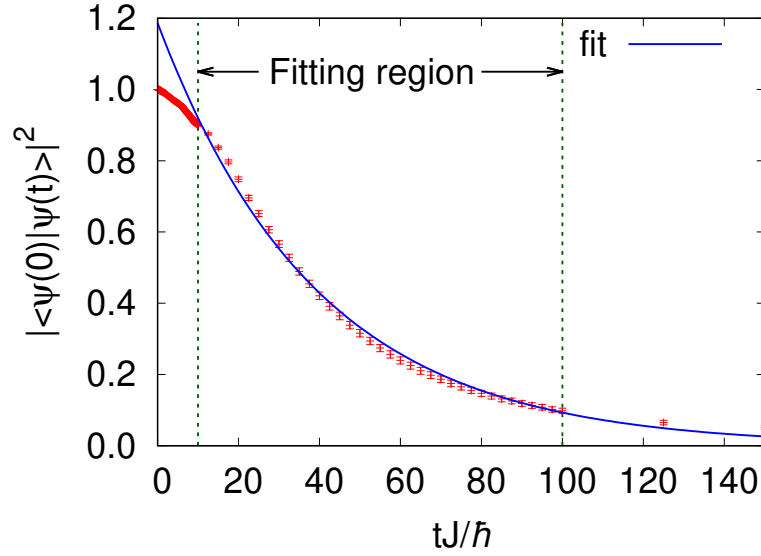


FIG. 8: Averaged fidelity for $M = N = 10$, $V = 0.1J$, and $W = 0.1J$. In this case, the fitting region is $10\hbar/J \leq t \leq 100\hbar/J$. The solid blue line represents the fit to a function $Ae^{-\Gamma t}$.

TABLE I: List of the values of the fitting region.

W/J	$t_1 J/\hbar$	$t_2 J/\hbar$
0.01	100	1000
0.03	100	300
0.1	10	100
0.3	5	30
1.0	0.5	1.5
3.0	0.2	1.0
10.0	0.1	0.5

* Electronic address: kunimi@rs.tus.ac.jp; Present address : Department of Physics, Tokyo University of Science, Shinjuku, Tokyo, 162-8601, Japan

† Electronic address: danshita@phys.kindai.ac.jp

[1] E. J. Torres-Herrera, M. Vyas, and L. F. Santos, New J. Phys. **16**, 063010 (2014).